The mammalian central nervous synaptic cleft contains a high density of periodically organized complexes

Benoît Zuber*†, Irina Nikonenko‡§, Paul Klauser‡, Dominique Muller‡, and Jacques Dubochet*

*Laboratoire d'Analyse Ultrastructurale, Bâtiment de Biologie, Université de Lausanne, CH-1015 Lausanne, Switzerland; and ‡Département de Neuropharmacologie, Centre Médical Universitaire, Université de Genève, 1 Rue Michel Servet, CH-1211 Geneva 4, Switzerland

Communicated by David J. DeRosier, Brandeis University, Waltham, MA, November 3, 2005 (received for review July 22, 2005)

Cryo-electron microscopy of vitreous section makes it possible to observe cells and tissues at high resolution in a close-to-native state. The specimen remains hydrated; chemical fixation and staining are fully avoided. There is minimal molecular aggregation and the density observed in the image corresponds to the density in the object. Accordingly, organotypic hippocampal rat slices were vitrified under high pressure and controlled cryoprotection conditions, cryosectioned at a final thickness of ≈70 nm and observed below −170°C in a transmission electron microscope. The general aspect of the tissue compares with previous electron microscopy observations. The detailed analysis of the synapse reveals that the density of material in the synaptic cleft is high, even higher than in the cytoplasm, and that it is organized in 8.2-nm periodic transcleft complexes. Previously undescribed structures of presynaptic and postsynaptic elements are also described.

Cryo-electron microscopy of vitreous section | high-pressure freezing | hippocampus

Synapses of the central nervous system (CNS) play a key role in neuronal information processing. Their physiology and structural organization have been extensively characterized (1, 2). The presynaptic compartment contains synaptic vesicles (SVs) filled with neurotransmitters. There is an intensive tethering and fusion activity between SVs and the presynaptic membrane. The postsynaptic membrane is covered with neurotransmitter receptors, which detect variations in neurotransmitter concentration. Postsynaptic submembrane cytoplasm is occupied by a complex network of proteins, the postsynaptic density, which modulates the strength of synaptic transmission. The space between both cells is the synaptic cleft. It contains neurotransmitter receptors and various adhesion molecules, such as N-cadherin and neural cell adhesion molecule. Their function in synapse formation and regulation is only beginning to be understood, and their precise spatial organization remains unclear (3).

Resolving the molecular structure of the synapse is difficult because, on one hand, high resolution x-ray diffraction data are obtained outside their cellular context (4, 5). On the other hand, conventional electron microscopy generally fails to resolve individual proteins in their natural environment because the preparation relies on chemical fixation, dehydration, resin-embedding, and heavy-metal staining and, thus, produces aggregation artifacts and artificial contrast, resulting in a limited resolution and a difficulty of interpreting the nature of the observed structures (6, 7). Freeze substitution and freeze etching, by which the specimen is immobilized by freezing and dehydrated at low temperature before being embedded in resin or replicated, were developed to reduce preparation artifacts but, even under these conditions, aggregation cannot be completely avoided. Depending on the protocols used for specimen preparation, the synaptic cleft presents different aspects. A dense central plaque was observed in some studies; in others, fibrils running parallel to the membranes or bridging both membranes were seen (2, 8–10). In several cases, these transsynaptic fibrils seem to be regularly spaced, with a reported period ranging from 6 nm to 22 nm (11). Presynaptic elements adjacent to SVs and plasma membranes also appear with different aspects. In most cases, they are fuzzy but there are also observations of a regular organization (12–14).

A major step toward overcoming preparation artifacts of conventional electron microscopy was the introduction of cryo-electron microscopy of thin film of vitrified suspension. It consists of cooling a thin layer of solution (<1 μm) so rapidly that water is immobilized before ice formation takes place. The specimen is then observed at low temperature in its fully hydrated state, generally without any additional stain (15, 16). Under these conditions, molecules have no opportunity to aggregate. Structures are preserved down to atomic resolution, and the observed contrast is directly related to density variations in the sample. The method, however, only works for particles or cells that can be squeezed in a sub-micrometer-thick vitreous film.

Cryo-electron microscopy of vitreous section (CEMOVIS) was developed to extend the advantage of vitrification to any cell and tissue (7, 16–21). In general, high-pressure cooling is used to vitrify samples of several hundred-micrometer thickness with minimal addition of cryoprotectant (22). Ultra-thin vitreous sections are then cut at a temperature never exceeding −140°C. They are observed in a cryo-electron microscope.

In the present work, we have used CEMOVIS to study the central nervous system. We have observed rat organotypic hippocampal slices, a convenient model system rich in synapses and very similar to original hippocampus (23). We have focused our observations on the structure of the synapse. Our major findings are that the density of material in the synaptic cleft is high, even higher than in the cytoplasm, and that it is organized in 8.5-nm periodic transsynaptic complexes. One should note that cryosections of CNS were obtained in ref. 24, but they were dried before observation because the goal was to localize ions. They were not meant to resolve high-resolution structure.

Materials and Methods

Slices Culture. Transverse hippocampal slices (400-μm thick) were prepared from 6- to 7-day-old rats and maintained 10–15 days in culture as described in ref. 23. During culture, slice thickness reduces by a factor of 2 or more (25).

High Pressure Freezing, Cryosectioning, and Cryo-Electron Microscopy. The standard cryofixation procedure for tissues used in our laboratory had to be modified to lead to successful vitrification

Conflict of interest statement: No conflicts declared.

Abbreviations: ACSF, artificial cerebrospinal fluid; CEMOVIS, cryo-electron microscopy of vitreous sections; SV, synaptic vesicle.

†To whom correspondence should be addressed. E-mail: benoit.zuber@unil.ch.

§Present address: Département de Biologie Cellulaire et de Morphologie, Université de Lausanne, 9 Rue du Bugnon, CH-1005 Lausanne, Switzerland.

© 2005 by The National Academy of Sciences of the USA

www.pnas.org/cgi/doi/10.1073/pnas.0509527102

of nervous tissue (26). A 1-mm-diameter disk corresponding to the CA3-CA1 region was punched out of the hippocampal organotypic slice and immediately immersed for 5 min in an artificial cerebrospinal fluid (ACSF) containing 124 mM NaCl, 1.2 mM KCl, 2.5 mM $CaCl_2$, 1.5 mM $MgCl_2$, 24 mM $NaHCO_3$, 1.2 mM $KH2PO_4$, 10 mM glucose, and 2 mM ascorbic acid at pH 7.4, supplemented with 20% dextran (wt/vol; average molecular mass 42 kDa; Sigma-Aldrich, Buchs, Switzerland) and 5% sucrose (146 mM) acting as cryoprotectant. The measured osmolarity of this solution is 600 mOsm. The disk was then vitrified in a HPM 010 high-pressure freezer (Bal-Tec, Balzers, Liechtenstein) at 2,000 bar (raising time 15 ms) and at an estimated cooling speed of 5,000 K/s at a 100-μm depth (27).

Vitreous sections were obtained as described in Norlen *et al.* (28) with the following modifications: cutting speed was set to 1 mm/s, and sections were transferred on carbon-covered 1000 Mesh copper grids (Agar Scientific, Essex, U.K.). Grids were transferred to a Gatan Cryoholder (Gatan, Warrendale, PA) kept at a temperature below −170°C, and inserted in a CM100 cryo-electron microscope (Philips, Eindhoven, The Netherlands) equipped with LaB_6 cathode. The accelerating voltage was either 80 or 100 kV. Specimens were irradiated with a low-electron dose. Electron diffraction was used to check whether water was vitreous or crystalline. Images were recorded with a TemCam-F224HD charge-coupled device camera (Tietz Video and Image Processing Systems, Munich) at magnifications ranging from 6,500× to 22,500×. No image processing other than that described in figure legends was performed. Actual section thickness was calculated as described in ref. 26. Sections kept for analysis were between 70 and 100 nm thick.

Dimension Measurements. Microscope magnifications were calibrated by using a 2D crystal of catalase (Agar Scientific). Dimension measurements are given with standard deviation and n, the number of measurements. During cryosectioning, material is compressed along the cutting direction parallel to the knife marks. Consequently, a circular body becomes elliptical after sectioning. The large axis of the ellipse, perpendicular to the cutting direction, remains constant, whereas there is a reduction along the cutting direction, compensated for by a proportional increase of the section thickness (29). Compression (c) was calculated from the equation

$$c = 1 - (d1/d2), \quad [1]$$

where $d1$ and $d2$ are, respectively, the small and large axes of the ellipse measured on many SVs. Average compression is 0.22 ± 0.08 ($n = 19$). Size measurements in the synapse were corrected for compression according to the equation

$$d = d'(1 + c\cos(\alpha)), \quad [2]$$

where d' and d are, respectively, the measured and corrected dimensions, c is the compression and α is the angle between the measured dimension and the cutting direction.

Conventional Electron Microscopy. To test the effect of the cryoprotectant, slices immersed in ACSF, supplemented and unsupplemented with 20% dextran and 5% sucrose for 10 min, were fixed for 1 h in 3% glutaraldehyde in 0.1 M phosphate buffer at pH 7.4, and further processed for conventional plastic embedding (30). Sections cut from the middle portion of the apical arborisation of CA1 pyramidal neurons were analyzed.

Electrophysiological Recordings. For recordings of field excitatory postsynaptic potentials (EPSPs), slices were placed in a recording chamber and continuously superfused with ACSF saturated with 95% O_2 and 5% CO_2 at a flow rate of 1 ml/min and at a temperature of 30°C. EPSPs were evoked by stimulation of a group of Schaffer collaterals and recorded in the stratum radiatum of the CA1 region by using patch pipettes filled with ACSF and recorded with an Axoclamp 2B (Axon Instruments, Foster City, CA). To test the effects of the cryoprotectant solution, the perfusion was switched for 8 min to an ACSF supplemented with 20% dextran and 5% sucrose and then returned to control ACSF while continuously monitoring synaptic responses.

Results

Establishment of the Best Freezing Conditions. Nervous tissue is more difficult to vitrify than any other tissue studied so far in our laboratory. Perhaps because nervous tissue has a higher water content (31), its intrinsic cryoprotective effect is insufficient. Because vitrification is a prerequisite for successful CEMOVIS, we have tested various cryoprotection conditions aimed at slightly decreasing neuronal water content by adding an osmotically active compound to the medium. We have found that immersion of a hippocampal organotypic brain slice in ACSF supplemented with 5% sucrose and 20% dextran for 5 min before freezing is the minimum requirement to achieve reproducible vitrification. Note that 20% dextran is routinely used for extracellular cryoprotection of cell suspension because it produces minimal osmotic effect (17–19).

Preservation of Synaptic Structure and Transmission: Slice Survival. We checked the possible effect of cryoprotectant on the structure of the nervous tissue by comparing uncryoprotected and cryoprotected samples prepared by conventional plastic embedding for transmission electron microscopy. The width of synaptic cleft is 19.3 ± 0.3 nm ($n = 73$) in the uncryoprotected sample and 19.6 ± 0.3 nm ($n = 60$) in the cryoprotected one. The diameter of SVs is 33.2 ± 0.1 nm ($n = 672$) in the control and 33.0 ± 0.1 nm ($n = 535$) in the cryoprotected sample. Although these synaptic structures are unaffected by the treatment, the cytoplasm appears denser in cryoprotected samples (data not shown). This observation agrees with our hypothesis that cryoprotectant treatment reduces cellular water content.

We also verified whether the cryoprotectant treatment affects the survival of slice cultures by monitoring evoked synaptic activity in the CA1 area before, during, and after the treatment. Consistent with observations in ref. 32, the cryoprotectant treatment results in a decrease of excitatory field potentials during perfusion (mean decrease: 51.7 ± 4.7%; $n = 4$), but recovery is complete within 15 min of reperfusion with control saline (99.4 ± 7.1%; $n = 4$). Thus, slices remain functional, and no long-term modification of the strength of synaptic transmission is observed.

General Aspect of Hippocampal Cryosections. A low-magnification view of an unstained vitreous section of hippocampus is presented in Fig. 1. The general histology is similar to fixed, dehydrated, and stained samples (see Fig. 1 legend; ref. 23). Membranes are well preserved and are 5.4 ± 0.4 nm thick ($n = 11$). It is not possible to trace them all around cells because they appear with high contrast only when they are aligned with the viewing direction. Presynaptic cytoplasm is populated with SVs. Cell shape is smoother and less angulated than in conventional sections but is similar to samples prepared by freeze substitution (8, 9, 25). Cryosections are prone to severe cutting artifacts (29). Knife marks and cutting direction are indicated by arrows. Compression along the cutting direction seems relatively homogeneous. It causes the elliptical shape of most vesicles and microtubules. It has been shown that compression does not affect dimensions measured perpendicularly to the cutting direction (16). Under our cutting conditions, it

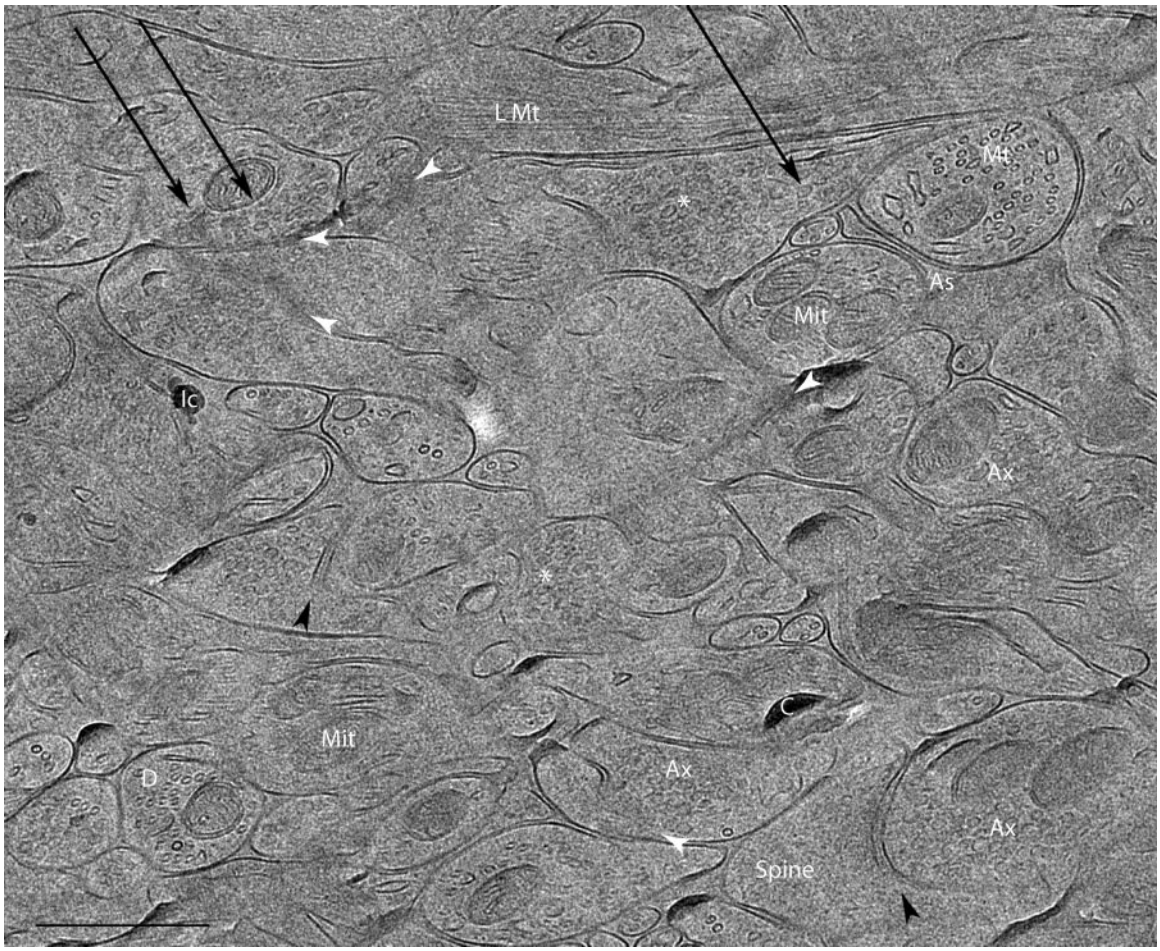

Fig. 1. Low-magnification view of an unstained vitreous section showing cellular projections. Cross-sectioned axons (Ax) contain SVs (*), whose size and shape are homogenous. Bundles of longitudinal microtubules (LMt) and cross-sectioned ones (Mt) are visible in many dendrites (D). Astrocytic processes (As) are very thin and tortuous cellular projections. At this magnification, synapses (black arrowheads) are characterized by an enlarged space with a thin dense line in the middle. One of the synapses contacts a dendritic spine, recognizable by its cup shape and the absence of microtubules in its cytoplasm (bottom right). Putative synapses, whose plasma membranes are not aligned along the viewing direction, are shown by white arrowheads. The mitochondria (Mit) matrix is denser than the cytoplasm. Black arrows, knife marks; C, crevasses; Ic, contaminating ice flake on the section. (Scale bar: 500 nm.)

was possible to avoid chatter and to limit crevasses to a few fractures along membranes.

Fig. 2 helps to interpret the contrasts observed in Fig. 1. It is a simple model of a vitreous section containing an SV, a microtubule seen along the viewing direction, and membranes in various orientations. Fig. 2*B* shows the expected optical density of the image. Because electron micrographs are noisy by nature, noise has been added in the simulation. It is apparent that an SV is far less contrasted than a microtubule seen in the optimal orientation and that membranes are clearly visible only when they are aligned along the viewing direction. In an SV, only the equatorial region is well contrasted.

Two typical synapses are shown in Figs. 3 and 4. Fig. 3 is close to focus. Its contrast is representative of density variations in the specimen. (*i*) It shows the shared features of synapses observed by CEMOVIS, conventional methods, and freeze substitution (2, 9). (*ii*) Presynaptic cytoplasm is filled with SVs (*). (*iii*) Extracellular volume is enlarged in the synaptic cleft. (*iv*) Postsynaptic density is found beneath the postsynaptic membrane at the level of the cleft (arrow). (*v*) Presynaptic density adjacent to the plasma membrane is frequently observed (white arrowhead). (*vi*) Mitochondria, which are recognizable from their double membrane (double black arrowhead) often surround the SV pool. Microtubules never penetrate this pool deeply.

Synaptic Features Revealed by CEMOVIS. CEMOVIS also reveals a number of features that have not previously been clearly identified or have appeared differently. The average diameter of SVs determined on this and similar micrographs is 37.7 ± 5.2 nm (n = 71). Mitochondria density is high. The various zones of the

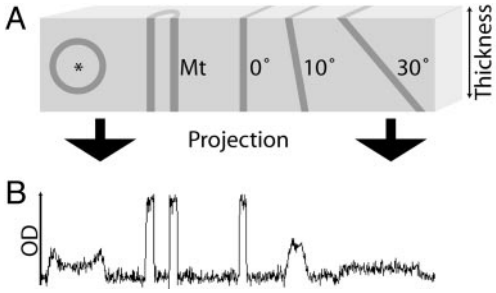

Fig. 2. Contrast formation in micrographs of unstained frozen-hydrated vitrified sections. (*A*) Schematic view of a section containing an SV (*), a cross-sectioned microtubule (Mt), a membrane aligned in the viewing direction, and two membranes tilted by 10° and 30°, respectively. The section thickness is 70 nm. (*B*) Optical density expected from a micrograph of the above section.

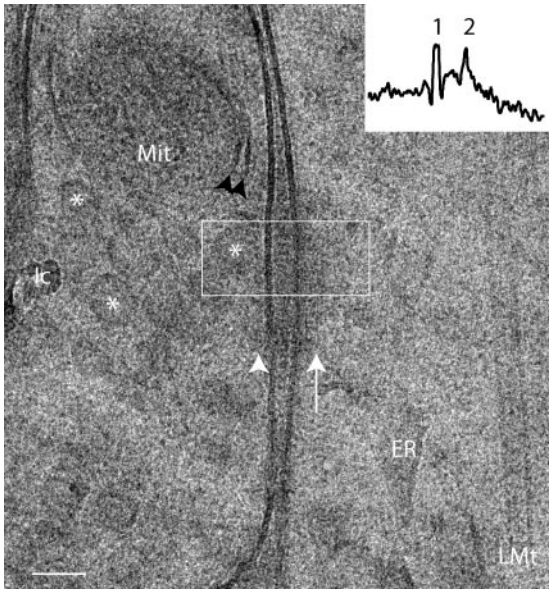

Fig. 3. Synapse recorded at 2,300 nm underfocus. Some SVs are indicated by an asterisk. Mit, mitochondrion; double black arrowhead, mitochondrial envelope; white arrowhead, presynaptic dense particles in close contact with the plasma membrane. In particular, one of the presynaptic dense particles makes contact with an SV (in the rectangle). Arrow, postsynaptic density; ER, twisted membranous cisternae, possibly of endoplasmic reticulum origin; LMt, longitudinal microtubule; Ic, ice contamination. (*Inset*) After Gaussian noise reduction, the mean density trace of the white rectangle was calculated. 1 and 2 are peaks corresponding to presynaptic and postsynaptic plasma membranes, respectively. (Scale bar: 50 nm.) Pixel size: 0.63 nm. First zero of the contrast transfer function: 2.9 nm.

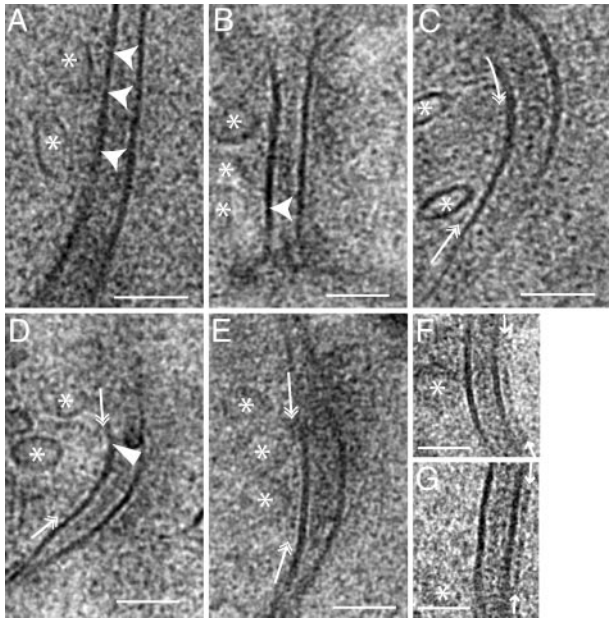

Fig. 5. Gallery of synaptic densities. (*A–E*) Presynaptic densities. Some SVs are indicated by an asterisk. Arrowhead, presynaptic dense granular particles; triangle, presynaptic dense fibrillar particle; between double headed arrows, presynaptic thin line. (*F* and *G*) Postsynaptic dense sheet; between arrows, thin postsynaptic line. All images have been denoised with a Gaussian blur of 1 pixel radius. (Scale bar: 50 nm.) Pixel size of *A*, *C*, *F*, and *G*, 0.63 nm; *B*, *D*, and *E*, 0.78 nm. Defocus (in nm): *A*, 2,900; *B*, 3,700; C, 3,400; *D*, 3,900; *E*, 2,700; *F*, 3,600; *G*, 3,900. First zero of the contrast transfer function (in nm): *A*, 3.3; *B*, 4.1; *C*, 3.6; *D*, 4.4; *E*, 3.1; *F*, 3.7; *G*, 4.

synapse seem to contain fine structures in the 10-nm range and below. Granules and filament-like structures are characteristic of the presynaptic zone. They frequently seem to be associated with SVs, and many are localized along the plasma membrane (Fig. 3, white arrowhead). One must, however, realize that such structures are difficult to interpret because they result from the superposition of features over the ≈70-nm thick section. The postsynaptic region is generally smoother. The width of the synaptic cleft, measured from membrane-to-membrane surfaces and corrected for compression (see *Materials and Methods*), is 23.8 ± 2.0 nm (n = 19). The broad synaptic zone is limited by regions of narrow (5.6 ± 1.3 nm (n = 15)], extracellular space. The density inside the synaptic cleft is higher than in the cytoplasm. It is comparable to, or even higher than, its level in mitochondria. The density in the extracellular space decreases outside the synaptic cleft. An averaged density scan obtained from the white-boxed zone is presented as *Inset*. It shows the irregular structure of the presynaptic zone, the sharp membranes, the high density of the cleft reaching its maximum in the middle, and the decreasing density of the postsynaptic side (corresponding to the white arrow). Most remarkable is the nonhomogeneous distribution of material in the synaptic cleft, where 5–10 nm of roughly regular patches of material seem to be concentrated toward the center of the cleft (upper half of the white box).

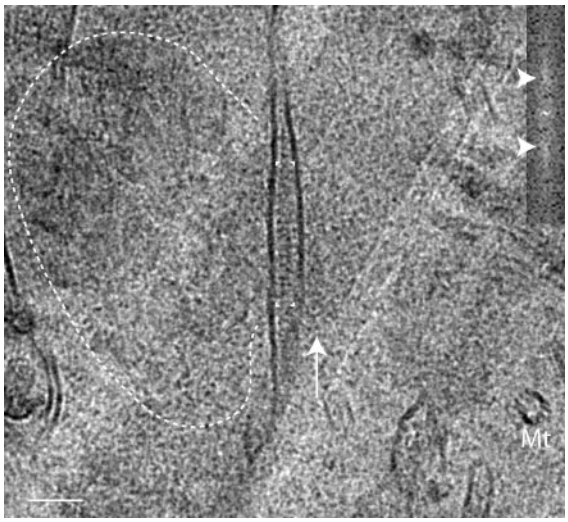

Fig. 4. Periodical organization of cleft complexes at 4,300 nm underfocus. This image has been denoised with a Gaussian blur of 1 pixel radius. The dashed line surrounds the SV pool. Arrow, postsynaptic density; Mt, microtubule. (*Inset*) Fourier transform of the nondenoised (i.e., raw image) region corresponding to the zone between rectangle corners. Arrowhead, position of the highest peak. (Scale bar: 50 nm.) Pixel size: 0.63 nm. First zero of the contrast transfer function: 4.2 nm.

Periodic Organization of the Cleft Complexes. Fig. 4 is defocused by 4,300 nm to best reveal structures in the 5–10 nm range. It seems very noisy in the presynaptic and postsynaptic zone, but it clearly shows the periodic arrangement of the material in the cleft. Because of the superposition effect, it is expected that such a periodic arrangement along the cleft is only visible in a minority of the synapses. The diffractogram of the marked zone (Fig. 4, white rectangle corners) demonstrate the strong periodic signal centered at 7.6 nm (arrowhead). From measurements over 14 synapses, and after correction for compression (see *Materials and Methods*), the periodicity along the synaptic cleft is found to be 8.2 ± 0.4 nm. Fig. 4 confirms the high density of material in the cleft, but the postsynaptic density is less marked than in many

other cases. It appears only as a slightly denser ≈15-nm layer adjacent to the postsynaptic membrane (white arrow).

Presynaptic and Postsynaptic Elements. Fig. 5 is a gallery of synapses at different defocus showing various features that are frequently observed. Cytoplasmic presynaptic structures resembling granules or fibers (Fig. 5 *A–E*; arrowheads and triangle, respectively) are frequently associated with SVs (*). We cannot decide whether the very thin line adjacent to the presynaptic membrane at ≈5 nm (Fig. 5 *C–E*; between double headed arrows) is an extremely thin nearly continuous layer or the superposition of numerous small granules. A similar layer on the postsynaptic side (Fig. 5 *F* and *G*; between arrows) is more contrasted. Its strongly granular nature suggests an aligned superposition of granules of <5 nm.

Discussion

CNS excitatory synapses are central to cerebral functions, but their structure is still not well known. Their cleft is most often regarded as an unstructured aqueous extracellular space. Many observations have shown that the reality is quite different, but no consensus has yet been reached about the structure of the various synaptic elements. In the cleft, a dense central plaque, fibrils running parallel to the membranes, and disorganized or periodically arranged transsynaptic fibers were observed, depending on preparation conditions (2, 9–11).

In our study, synapses are in a better state of preservation: We have vitrified living organotypic hippocampal slices from rats and observed them hydrated and unstained. Molecular aggregation is minimized and the observed optical density of the image directly correlates with matter density in the specimen (7). Ideally, nervous tissue should be cryofixed without any cryoprotectant, as has been done for cartilage and skin (26–28, 33). Unfortunately, this process has not yet been possible. However, we have shown by conventional electron microscopy that the structure of the synapse is not visibly affected by a brief incubation in 20% osmotically nonactive dextran, supplemented with the minimal amount of 5% sucrose. Moreover, recordings of evoked synaptic activity show no lasting modifications after treatment with the cryoprotectant, demonstrating that organotypic hippocampal slices stay alive and synapses remain functional. We have also to keep in mind that, even if vitrification is orders of magnitude more rapid than chemical fixation, it takes in the range of 10 ms to immobilize the sample (27). This duration is not negligible in comparison with synaptic events. Furthermore, the sudden application of high pressure may influence synaptic structures.

Excitatory and inhibitory synapses differ in several aspects; in particular, the former are larger than the latter (2). Based on this criterion, all of the synapses shown in the present study are likely to be of the excitatory type. The most striking feature that we have observed is the 8.2-nm periodic organization of the cleft complexes. As expected, it is observed only in a minority of the synapses because it must have the right orientation, but our observation is compatible with its presence in every synapse. Because CEMOVIS micrographs are made by the superposition of features over 70 nm, it is difficult to interpret the 3D organization of the periodic complexes. The repeated motif could be either a single layer or several superimposed filaments. In any case, they must be regularly arranged. Although the identity of the complexes cannot be stated, a number of data suggest that they could be made of a variety of adhesion molecules, which are widely expressed at the synapse (3). From the atomic map of two homophilic adhesion molecules, N-cadherin (4) and neural cell adhesion molecule (5), a zipper organization keeping presynaptic and postsynaptic membranes aligned has been hypothesized (4, 5). The expected period is ≈7.5 nm for N-cadherin and ≈8 nm for neural cell adhesion molecule. Our observations are compatible with this model. Moreover, the center of the cleft is denser, suggesting that molecules arising from both plasma membranes overlap to close the zipper. Recently, Lucic *et al.* (34) have observed isolated synaptosomes in thin vitrified layer. A 3D model of the cleft has been reconstructed and reveals a more complex and highly connected molecular network. Structural damage or loss of material associated with the preparation of the synaptosomes could explain the difference with our observations.

The structure of skin desmosome, a cadherin-based cell-cell junction, was recently revealed by CEMOVIS (26). Its extracellular component is characterized by a 5-nm periodic straight transverse structure, which appears more regular than the synaptic cleft complexes. This difference is consistent with the lesser diversity of desmosomal proteins, and with the fact that synapses not only have adhesive properties to keep presynaptic and postsynaptic elements aligned, but also possess more elaborate and dynamic functions. Accordingly, we might conceive subtle modifications of the structure of the synaptic cleft, in relation to synaptic plasticity. Another important issue is the fate of the organized cleft structure in relation to SV fusion with presynaptic plasma membrane. Depending on the model considered (kiss-and-run or complete fusion), this event could generate a considerable movement of phospholipids, which have to be accommodated with the structure in the cleft.

CEMOVIS makes it possible to determine the real density of even the smallest cell compartments. It reveals that the concentration of material in the cleft is higher than in the cytoplasm. This observation definitely makes obsolete the widespread conception of a simple prolongation of the extracellular space. Consequently, neurotransmitters might not be able to diffuse as freely as was previously thought, and computer simulation-based models will have to incorporate these data (35–37). Similarly, postsynaptic neurotransmitter receptor diffusion, which is implied in synaptic plasticity (38), might be affected by the organized complexes.

Presynaptic granules or fibers are frequently observed close to SVs and to the plasma membrane. They could be part of the cytoskeletal matrix assembled at the active zone of neurotransmitter release (39). On 2D images, it is difficult to characterize these structures more precisely, but our data prove that these structures do exist and raise the hope that tomography of vitreous sections will allow their detailed characterization. Currently, technical problems still prevent the routine use of tomography of vitreous sections, but encouraging results have already been published by Lucic *et al.* (34) and Hsieh *et al.* (40).

Postsynaptic densities can be classified into two categories. The first is represented by a density fading over some tens of nanometers. It corresponds to the postsynaptic density described with conventional electron microscopy (Figs. 3 and 4; refs. 2 and 13). The second category is formed by a 5-nm-thick sheet (Fig. 5 *F* and *G*). More investigation is needed to define the nature and role of this sheet. Dosemeci *et al.* (41) showed that synaptic activity leads to a transient thickening of the postsynaptic density. Accordingly, we can speculate that the two observed forms might correspond to two different functional states. Alternatively, they could represent two distinct classes of synapse.

The dimensions of several features appear larger with CEMOVIS than with conventional electron microscopy. For example, the average diameter of SVs is 37.7 nm in the hydrated state, whereas in conventional dehydrated sections it is between 30.4 and 35.2 nm (42, 43). Similarly, the cleft width of excitatory synapses is ≈20 nm in conventional sections (2, 43), whereas in cryosections, it is 23.8 nm. This result is consistent with the 24.2-nm-wide cleft of isolated synapses studied by cryo-electron tomography (34). The dimensions obtained with cryomethods should be considered as closer to

reality because, contrary to conventional methods, they do not require dehydration, so that molecular aggregation and subsequent shrinkage are minimized (6, 7, 16).

In the future, we hope that improvements of high-pressure freezing and finer biopsy techniques will make it possible to vitrify small pieces of nervous tissue without the need for any cryoprotectant. Furthermore, tomography of vitreous sections, associated with computerized image processing, such as docking of proteins of known atomic structures in the tomograms, will lead to a molecular map of synaptic biochemical cycles and signaling pathways and catch transient complexes that could not be revealed by any other mean (44).

We thank L. Parisi and M. Moosmayer for culture preparation; A. Al-Amoudi for many helpful discussions and pieces of advice; H. Stahlberg and J. Evans for advice about image processing; and O. Shupliakov for helpful discussions and critical reading of the manuscript. This work was supported by the 3D-Electron Microscopy Network of the European Research Framework Program 6 (to J.D.) and Fonds National de la Recherche Scientifique Grant 105721 and the European Promemoria Project (to D.M.).

1. Cowan, W. M., Südhof, T. C. & Stevens, C. F. (2001) *Synapses* (Johns Hopkins Univ. Press, Baltimore).
2. Peters, A., Palay, S. & Webster, H. (1991) *The Fine Structure of the Nervous System* (Oxford Univ. Press, New York).
3. Yamagata, M., Sanes, J. R. & Weiner, J. A. (2003) *Curr. Opin. Cell Biol.* **15,** 621–632.
4. Shapiro, L., Fannon, A. M., Kwong, P. D., Thompson, A., Lehmann, M. S., Grubel, G., Legrand, J. F., Als-Nielsen, J., Colman, D. R. & Hendrickson, W. A. (1995) *Nature* **374,** 327–337.
5. Soroka, V., Kolkova, K., Kastrup, J. S., Diederichs, K., Breed, J., Kiselyov, V. V., Poulsen, F. M., Larsen, I. K., Welte, W., Berezin, V., Bock, E. & Kasper, C. (2003) *Structure (London)* **11,** 1291–1301.
6. Carlemalm, E., Villiger, W., Acetarin, J.-D. & Kellenberger, E. (1984) in *Science of Biological Specimen Preparation*, ed. Johari, O. (SEM Inc., AMF O'Hare, Chicago), pp. 147–154.
7. Dubochet, J. & Sartori Blanc, N. (2001) *Micron* **32,** 91–99.
8. Hirokawa, N. & Kirino, T. (1980) *J. Neurocytol.* **9,** 243–254.
9. Ichimura, T. & Hashimoto, P. H. (1988) *J. Neurocytol.* **17,** 3–12.
10. Landis, D. M. & Reese, T. S. (1983) *J. Cell Biol.* **97,** 1169–1178.
11. Elfvin, L. (1977) *Prog. Neurobiol.* **8,** 45–79.
12. Gray, E. G. (1963) *J. Anat.* **97,** 101–106.
13. De Camilli, P., Haucke, V., Takei, K. & Mugnaini, E. (2001) in *Synapses*, eds. Cowan, W. M., Südhof, T. C. & Stevens, C. F. (Johns Hopkins Univ. Press, Baltimore), pp. 89–133.
14. Phillips, G. R., Huang, J. K., Wang, Y., Tanaka, H., Shapiro, L., Zhang, W., Shan, W. S., Arndt, K., Frank, M., Gordon, R. E., *et al.* (2001) *Neuron* **32,** 63–77.
15. Adrian, M., Dubochet, J., Lepault, J. & McDowall, A. W. (1984) *Nature* **308,** 32–36.
16. Dubochet, J., Adrian, M., Chang, J. J., Homo, J. C., Lepault, J., McDowall, A. W. & Schultz, P. (1988) *Q. Rev. Biophys.* **21,** 129–228.
17. Matias, V. R., Al-Amoudi, A., Dubochet, J. & Beveridge, T. J. (2003) *J. Bacteriol.* **185,** 6112–6118.
18. Al-Amoudi, A., Norlen, L. P. & Dubochet, J. (2004) *J. Struct. Biol.* **148,** 131–135.
19. Zhang, P., Bos, E., Heymann, J., Gnaegi, H., Kessel, M., Peters, P. J. & Subramaniam, S. (2004) *J. Microsc. (Oxford)* **216,** 76–83.
20. Al-Amoudi, A., Chang, J. J., Leforestier, A., McDowall, A., Salamin, L. M., Norlen, L. P., Richter, K., Blanc, N. S., Studer, D. & Dubochet, J. (2004) *EMBO J.* **23,** 3583–3588.
21. Matias, V. R. & Beveridge, T. J. (2005) *Mol. Microbiol.* **56,** 240–251.
22. Dubochet, J. (1995) *Trends Cell Biol.* **5,** 366–368.
23. Stoppini, L., Buchs, P. A. & Muller, D. (1991) *J. Neurosci. Methods* **37,** 173–182.
24. Pozzo-Miller, L. D., Pivovarova, N. B., Leapman, R. D., Buchanan, R. A., Reese, T. S. & Andrews, S. B. (1997) *J. Neurosci.* **17,** 8729–8738.
25. Pozzo Miller, L. D. & Landis, D. M. (1993) *Synapse* **13,** 195–205.
26. Al-Amoudi, A., Dubochet, J. & Norlen, L. (2005) *J. Invest. Dermatol.* **124,** 764–777.
27. Studer, D., Michel, M., Wohlwend, M., Hunziker, E. B. & Buschmann, M. D. (1995) *J. Microsc. (Oxford)* **179,** 321–332.
28. Norlen, L., Al-Amoudi, A. & Dubochet, J. (2003) *J. Invest. Dermatol.* **120,** 555–560.
29. Al-Amoudi, A., Studer, D. & Dubochet, J. (2005) *J. Struct. Biol.* **150,** 109–121.
30. Skibo, G. G., Nikonenko, I. R., Savchenko, V. L. & McKanna, J. A. (2000) *Neuroscience* **96,** 427–438.
31. Schwab, M., Bauer, R. & Zwiener, U. (1997) *Brain Res.* **749,** 82–87.
32. Huang, R. & Somjen, G. G. (1995) *Brain Res.* **702,** 181–187.
33. Norlen, L. & Al-Amoudi, A. (2004) *J. Invest. Dermatol.* **123,** 715–732.
34. Lucic, V., Yang, T., Schweikert, G., Forster, F. & Baumeister, W. (2005) *Structure (London)* **13,** 423–434.
35. Trommershauser, J., Marienhagen, J. & Zippelius, A. (1999) *J. Theor. Biol.* **198,** 101–120.
36. Ventriglia, F. (2004) *Biol. Cybern.* **90,** 349–359.
37. Sykova, E. (2004) *Neuroscience* **129,** 861–876.
38. Choquet, D. & Triller, A. (2003) *Nat. Rev. Neurosci.* **4,** 251–265.
39. Dresbach, T., Qualmann, B., Kessels, M. M., Garner, C. C. & Gundelfinger, E. D. (2001) *Cell. Mol. Life Sci.* **58,** 94–116.
40. Hsieh, C. E., Marko, M., Frank, J. & Mannella, C. A. (2002) *J. Struct. Biol.* **138,** 63–73.
41. Dosemeci, A., Tao-Cheng, J.-H., Vinade, L., Winters, C. A., Pozzo-Miller, L. & Reese, T. S. (2001) *Proc. Natl. Acad. Sci. USA* **98,** 10428–10432.
42. Crowder, K. M., Gunther, J. M., Jones, T. A., Hale, B. D., Zhang, H. Z., Peterson, M. R., Scheller, R. H., Chavkin, C. & Bajjalieh, S. M. (1999) *Proc. Natl. Acad. Sci. USA* **96,** 15268–15273.
43. Schikorski, T. & Stevens, C. F. (1997) *J. Neurosci.* **17,** 5858–5867.
44. Sali, A., Glaeser, R., Earnest, T. & Baumeister, W. (2003) *Nature* **422,** 216–225.